Theoretical & Applied Mechanics Letters 7 (2017) 235–242

Contents lists available at ScienceDirect

Theoretical & Applied Mechanics Letters

journal homepage: www.elsevier.com/locate/taml

Letter

Entropy analysis in electrical magnetohydrodynamic (MHD) flow of nanofluid with effects of thermal radiation, viscous dissipation, and chemical reaction

Yahaya Shagaiya Daniel [a], Zainal Abdul Aziz [a,*], Zuhaila Ismail [a], Faisal Salah [b]

[a] UTM Centre for Industrial and Applied Mathematics, Universiti Teknologi Malaysia, 81310 UTM Johor Bahru, Johor, Malaysia
[b] Department of Mathematics, Faculty of Science, University of Kordofan, Elobid 51111, Sudan

HIGHLIGHTS

- Entropy generation and Bejan number on unsteady electrical magnetohydrodynamic (MHD).
- A similarity transformation solved by Keller box method is used then.
- Suction at the wall, electric and magnetic fields are taken into account.
- Effects of thermal radiation, viscous dissipation, chemical reaction are examined.

ARTICLE INFO

Article history:
Received 9 December 2016
Received in revised form 22 May 2017
Accepted 5 June 2017
Available online 21 June 2017
*This article belongs to the Solid Mechanics

Keywords:
Entropy generation
MHD nanofluid
Thermal radiation
Bejan number
Chemical reaction
Viscous dissipation

ABSTRACT

The unsteady mixed convection flow of electrical conducting nanofluid and heat transfer due to a permeable linear stretching sheet with the combined effects of an electric field, magnetic field, thermal radiation, viscous dissipation, and chemical reaction have been investigated. A similarity transformation is used to transform the constitutive equations into a system of nonlinear ordinary differential equations. The resultant system of equations is then solved numerically using implicit finite difference method. The velocity, temperature, concentration, entropy generation, and Bejan number are obtained with the dependence of different emerging parameters examined. It is noticed that the velocity is more sensible with high values of electric field and diminished with a magnetic field. The radiative heat transfer and viscous dissipation enhance the heat conduction in the system. Moreover, the impact of mixed convection parameter and Buoyancy ratio parameter on Bejan number profile has reverse effects. A chemical reaction reduced the nanoparticle concentration for higher values.

The magnetohydrodynamic (MHD) mixed convection flow and heat transfer due to stretching sheet in a uniform stream of fluid have received great attention lately, as a result of practical applications in industrial and engineering fields. These areas of applications cut across in metallurgy, aerodynamic extrusion of plastic sheet, extrusion of a polymer from a dye in the manufacturing industry, cooling of a metallic plate, cooling or drying of textile and glass fiber production. The level of stretching and cooling has momentous effects on the quality of the finished product with desired properties.

Nanofluids are being used to enhance the thermal conductivity of base fluids such as water, propylene glycol, and ethylene glycol. Suspending an ultrafine nanoparticle in a traditional fluid causes an enhancement in the thermal conductivity [1]. Kuznetsov and Nield [2] studied the natural convective boundary-layer flow of a nanofluid due to the vertical plate which incorporated Brownian motion and thermophoresis effects. Khan and Pop [3] extended the model to the boundary-layer flow of a nanofluid due to the stretching sheet with a constant surface temperature. An experimental investigation conducted by Haddad et al. [4] explored natural convection in nanofluid taking into account thermophoresis and Brownian motion in heat transfer enhancement. Their results revealed that neglecting the key role of Brownian motion and thermophoresis deteriorates the heat transfer which increases when the volume fraction of a nanoparticles upsurges.

* Corresponding author.
E-mail addresses: shagaiya12@gmail.com (Y.S. Daniel), zainalaz@utm.my (Z.A. Aziz), zuhaila@utm.my (Z. Ismail), faisal19999@yahoo.com (F. Salah).

http://dx.doi.org/10.1016/j.taml.2017.06.003

Nomenclature

a, b	Constants
B_0	Magnetic field factor
Be	Bejan number
Br	Brinkman number
c_f	Skin friction coefficient
C_∞	Ambient concentration
D_B	Brownian diffusion coefficient
D_T	Thermophoresis diffusion coefficient
E_0	Electric field factor
Ec	Eckert number
f	Dimensionless velocity
Ha	Hartmann number
J	Joule current
k	Thermal conductivity
Le	Lewis number
M	Magnetic field parameter
Rd	Radiation parameter
Nb	Brownian motion parameter
Nt	Thermophoresis parameter
Nu	Local Nusselt number
P	Fluid pressure
Pr	Prandtl number
q_r	Radiative heat flux
Re	Local Reynolds number
s	Suction/injection
Sh	Local Sherwood number
T	Temperature of the fluid
T_W	Constant temperature at the wall
T_∞	Ambient temperature
u, v	Velocity component along x- and y-direction
V_W	Wall mass transfer
V	Fluid velocity

Greek symbols

α	Thermal diffusivity
σ	Electrical conductivity
$\sigma*$	Stefan–Boltzmann constant
η	Dimensionless similarity variable
μ	Dynamic viscosity of the fluid
υ	Kinematic viscosity of the fluid
ρ_f	Density of the fluid
$(\rho c)_f$	Heat capacity of the fluid
$(\rho c)_p$	Effective heat capacity of a nanoparticle
ψ	Stream function
σ	Electrical conductivity
Σ	Dimensionless concentration difference
φ_W	Nanoparticle volume fraction at the surface
φ_∞	Nanoparticle volume fraction at large values of y
θ	Dimensionless temperature
ϕ	Dimensionless concentration
τ	Ratio between the effective heat transfer capacity and the heat capacity of the fluid
λ	Mixed convection parameter
Ω	Dimensionless temperature difference
γ	Chemical reaction parameter

Subscripts

∞	Condition at the free stream
W	Condition at the surface

Magnetic nanofluid is a colloidal suspension of carrier magnetic nanoparticles and liquid. Diverse kinds of physical features of these fluids can be tuned through the varying magnetic field. The magnetic nanofluids are controlled by an external magnetic field, which has been used for different investigation. The investigation of the MHD flow of an electrically conducting fluid over a stretching sheet is important in modern metallurgy and metal working mechanism. Investigation by Hayat et al. [5] have shown that the rate of heat transfer is enhanced by increasing the strength of magnetic field. Reduction of Nusselt number as result of magnetic field dependent (MFD) viscosity influence are more sensible for low Hartmann number and high Rayleigh [6]. It will be appropriate to consider not only the single phase model but the two-phase approach discussed by Sheikholeslami and Ganji [7], which seems a better model to show nanofluid flow due to slip velocity mechanism between the base fluid and the nanoparticle which play a vital role in the heat transfer performance of nanofluid. Das et al. [8] indicate that magnetic field enhances the nanofluid velocity in the channel. Farooq et al. [9] showed that skin friction rises for higher magnetic fields. Enhancement in heat transfer have a direct relationship with the Hartmann and Reynolds numbers, but an inverse relationship with the magnetic field [10]. Also, the Nusselt number is an increasing function of nanoparticle volume fraction and magnetic field. Nanoparticle fraction rises as the rate of mass transfer from the sheet reduces and thermophoresis increases [11]. Sheikholeslami and Ellahi's [12] work revealed that applying magnetic field results in a force opposite to the flow direction which leads to a drag in the flow and decrease in the convection currents by reducing the velocity. Some others researchers did interesting investigations in this direction [13–19].

The thermal radiation influence plays a key role in the industrial and engineering processes. These processes involve performance at an extreme temperature under different non-isothermal conditions and instances where convective heat transfer coefficients are lower. Radiative heat transfer is used in the model of pertinent, equipment, hypersonic flights, nuclear reactors, nuclear power plants, space vehicles, gas turbines, etc. The temperature field enhanced for rising temperature ratio and radiation in copper–water nanofluid as presented by Hayat et al. [20], silver nanofluid dominant for skin friction as copper nanofluid dominant over silver nanofluid for the local Nusselt number. The higher range of values of non-linear thermal radiation seen by Hayat et al. [21] resulted in the enhancement of temperature field. The numerical results of Sheikholeslami et al. [22] showed that coefficient of skin friction enhances with increasing magnetic field whereas decreases with the rise in velocity ratio. The Nusselt number has a direct dependence on the temperature index and velocity ratio but reverse dependence for radiation and magnetic fields. Hayat et al. [23] showed that heat transfer rate enhances when temperature and radiation increase.

The application of magnetic field in electric conducting nanofluid has drawn the attention of researchers currently. The results of Sheikholeslami et al. [24] showed that electric field on heat transfer is more pronounced at smaller Reynolds number. Sheikholeslami and Chamkha [25] indicate that the impact of electric field on heat transfer is as a result of the predomination of the conduction mechanism, which makes it more pronounced. Suction/blowing of nanofluid by the boundary mass transfer can significantly alter the flow field. Suction tends to increase the skin friction, as blowing behave in reserve manners. The process of suction/blowing plays a dominant role in the design of radial diffusers and thrust bearing, thermal oil recovery, etc., which is of importance to the areas of engineering. Suction/injection has (blowing) been reported by many other researchers in Refs. [26–30].

Entropy generation minimization approach, as a thermodynamic is used to optimize the thermal engineering devices for

better energy efficiency [31]. The enhancement of engineering equipment devices is due to irreversibilities [32]. Entropy generation measures the rate of available irreversibilities in a process. It makes more emphasis on the second law of thermodynamics than the first law, due to the limitation in heat transfer system. In heated inclined plate base on the work of Adesanya and Makinde [33] increases with a rise in viscosity, couple stress inverse, and viscous heating. Heat transfer irreversibility dominates over fluid friction irreversibility with the increase of such parameters. Consequently, the dominant impact of heat transfer and nanoparticle mass transfer irreversibilities rises [34]. Bejan number is an increasing function of viscosity, whereas is the decreasing function of other active involves parameters. Nusselt number reduces with the rise of thermal radiation, thermophoretic, Brownian motion, and viscous dissipation [35–38].

Most of the investigations on unsteady MHD mixed convection flow of nanofluid due to stretching sheet and heat transfer with effects of Brownian motion and thermophoresis do not incorporate the combined impact of thermal radiation, electrical field, chemical reaction, and viscous dissipation in entropy generation. Bejan number has not been considered by the researchers. Due to motivation on the need to crisp the understanding of the second law of thermodynamic analysis. This analysis is carried out in order to enhance the system performance, with the aforementioned used as a source of entropy generation on unsteady electrical MHD mixed convection flow of nanofluid due to a linear permeable stretching sheet with water based nanofluid [39] is used which is a novel. Implicit finite difference scheme presented in Cebeci and Bradshaw [40] is employed to solve the problem. The influence of entropy generation and Bejan numbers is investigated and shown in detail. The influence of physical parameters on velocity, temperature, particle concentration, entropy generation number, and Bejan number of nanofluid has been discussed extensively and presented graphically.

In this paper, we consider the unsteady mixed convection flow of an electrically conducting viscous incompressible nanofluid with combined impacts of thermal radiation, chemical reaction, and viscous dissipation over a stretching sheet in the presence of electric field. The sheet is stretched with velocity $u_W(x,t)$, which varies with time t as well as the distance along the sheet from the origin x, with two equal and opposite forces are spontaneously applied. The schematic sketch of the problem is presented in Fig. 1. The coordinate system is chosen in such a way that x-axis is measured along the stretching sheet, y-axis is normal to it and the flow is occupied above the surface $y > 0$. The applied magnetic field B and electric field E are implemented in the positive y-direction. The surface temperature $T_W(x,t)$ and surface concentration $\varphi_W(x,t)$ are assumed to be higher than the ambient temperature T_∞ and ambient concentration φ_∞. The induced magnetic field and Hall current effects are insignificant to small magnetic Reynolds number. Using Buongiorno model, the constitutive equations governing the flow are given as:

Continuity equation

$$\frac{\partial u}{\partial x}+\frac{\partial v}{\partial y}=0. \tag{1}$$

x-momentum equation

$$\begin{aligned}&\frac{\partial u}{\partial t}+u\frac{\partial u}{\partial x}+v\frac{\partial u}{\partial y}\\&=-\frac{1}{\rho_{\mathrm{f}}}\frac{\partial P}{\partial x}+\nu\left(\frac{\partial^2 u}{\partial x^2}+\frac{\partial^2 u}{\partial y^2}\right)+\frac{\sigma}{\rho_{\mathrm{f}}}\left(EB-B^2u\right)\\&\quad+\frac{1}{\rho_{\mathrm{f}}}\left[\left(1-\varphi_\infty\right)\rho_{\mathrm{f}\infty}\beta\left(T-T_\infty\right)\right.\\&\quad\left.-\left(\rho_{\mathrm{p}}-\rho_{\mathrm{f}\infty}\right)\left(\varphi-\varphi_\infty\right)\right]g.\end{aligned} \tag{2}$$

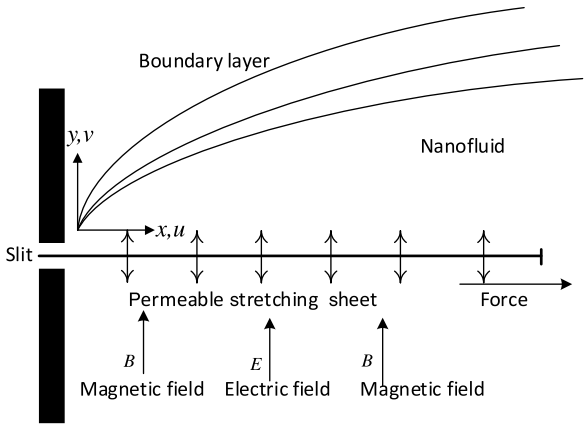

Fig. 1. Physical configuration of the geometry.

y-momentum equation

$$\begin{aligned}&\frac{\partial v}{\partial t}+u\frac{\partial v}{\partial x}+v\frac{\partial v}{\partial y}\\&=-\frac{1}{\rho_{\mathrm{f}}}\frac{\partial P}{\partial y}+\nu\left(\frac{\partial^2 v}{\partial x^2}+\frac{\partial^2 v}{\partial y^2}\right)+\frac{\sigma}{\rho_{\mathrm{f}}}\left(EB-B^2v\right)\\&\quad+\frac{1}{\rho_{\mathrm{f}}}\left[\left(1-\varphi_\infty\right)\rho_{\mathrm{f}\infty}\beta\left(T-T_\infty\right)\right.\\&\quad\left.-\left(\rho_{\mathrm{p}}-\rho_{\mathrm{f}\infty}\right)\left(\varphi-\varphi_\infty\right)\right]g.\end{aligned} \tag{3}$$

Energy equation

$$\begin{aligned}&\frac{\partial T}{\partial t}+u\frac{\partial T}{\partial x}+v\frac{\partial T}{\partial y}\\&=\frac{k}{(\rho c)_{\mathrm{f}}}\left(\frac{\partial^2 T}{\partial x^2}+\frac{\partial^2 T}{\partial y^2}\right)-\frac{1}{(\rho c)_{\mathrm{f}}}\left(\frac{\partial q_r}{\partial y}\right)+\frac{\mu}{(\rho c)_{\mathrm{f}}}\left(\frac{\partial u}{\partial y}\right)^2\\&\quad+\tau\left\{D_{\mathrm{B}}\left(\frac{\partial\varphi}{\partial x}\frac{\partial T}{\partial x}+\frac{\partial\varphi}{\partial y}\frac{\partial T}{\partial y}\right)+\frac{D_{\mathrm{T}}}{T_\infty}\left[\left(\frac{\partial T}{\partial x}\right)^2+\left(\frac{\partial T}{\partial y}\right)^2\right]\right\}.\end{aligned} \tag{4}$$

Concentration equation

$$\begin{aligned}&\frac{\partial\varphi}{\partial t}+u\frac{\partial\varphi}{\partial y}+v\frac{\partial\varphi}{\partial y}=D_{\mathrm{B}}\left(\frac{\partial^2\varphi}{\partial x^2}+\frac{\partial^2\varphi}{\partial y^2}\right)\\&\quad+\frac{D_{\mathrm{T}}}{T_\infty}\left(\frac{\partial^2 T}{\partial x^2}+\frac{\partial^2 T}{\partial y^2}\right)-k_1\left(\varphi-\varphi_\infty\right).\end{aligned} \tag{5}$$

The boundary conditions on the sheet for the physical model are presented by

$$\begin{aligned}y=0:\quad &u=u_w(x,t),\quad v=v_w(x,t),\\&T=T_W(x,t),\quad \varphi=\varphi_W(x,t),\end{aligned}$$

$$y\longrightarrow\infty:\quad u\to 0,\quad T\longrightarrow T_\infty,\quad \varphi\longrightarrow\varphi_\infty, \tag{6}$$

where $u_w(x,t)=bx/(1-at)$ denotes the velocity of the linear stretching sheet (b and a are positive constants with dimension T^{-1} having $1-at>0$), $v_w=-v_0/\sqrt{1-at}$ is the wall mass transfer, for $v_w<0$ denote the injection while $v_w>0$ indicates the suction. u and v represent the velocity components along the x- and y-axes respectively. As p, $\alpha=k/(\rho c)_{\mathrm{f}}$, μ, ρ, ρ_{f}, and ρ_{p} are the fluid pressure, thermal diffusivity, kinematic viscosity, density, fluid density, and particle density, respectively. We also have D_{B}, D_{T}, and $\tau=(\rho c)_{\mathrm{p}}/(\rho c)_{\mathrm{f}}$ which represents the Brownian diffusion coefficient, the thermophoresis diffusion coefficient, and the ratio between the effective heat transfer capacity of the ultrafine nanoparticle

material and the heat capacity of the fluid. $B = B_0/\sqrt{1-at}$ is the strength of magnetic field, $E = E_0/\sqrt{1-at}$ denotes the strength of electric field, and $k_1 = k_0/(1-at)$ represents the rate of chemical reaction.

The radiative heat flux q_r via Rosseland approximation [13] is applied to Eq. (4), such that

$$q_r = -\frac{4\sigma^*}{3k^*}\frac{\partial T^4}{\partial y}, \tag{7}$$

where σ^* represents the Stefan–Boltzmann constant and k^* denotes the mean absorption coefficient. Expanding T^4 by using Taylor's series about T_∞ and neglecting higher order terms, we have

$$T^4 = 4T_\infty^3 T - 3T_\infty^4. \tag{8}$$

Using Eq. (8) into Eq. (7), we get

$$\frac{\partial q_r}{\partial y} = -\frac{16T_\infty^3\sigma^*}{3k^*}\frac{\partial^2 T}{\partial y^2}. \tag{9}$$

Using Eq. (9) in Eq. (4), we obtain

$$\begin{aligned}\frac{\partial T}{\partial t} + u\frac{\partial T}{\partial x} + v\frac{\partial T}{\partial y} &= \frac{k}{(\rho c)_{\mathrm{f}}}\left(\frac{\partial^2 T}{\partial x^2} + \frac{\partial^2 T}{\partial y^2}\right) \\ &+ \frac{1}{(\rho c)_{\mathrm{f}}}\left(\frac{16T_\infty^3\sigma^*}{3k^*}\frac{\partial^2 T}{\partial y^2}\right) + \frac{\mu}{(\rho c)_{\mathrm{f}}}\left(\frac{\partial u}{\partial y}\right)^2 \\ &+ \tau\left\{D_{\mathrm{B}}\left(\frac{\partial \varphi}{\partial x}\frac{\partial T}{\partial x} + \frac{\partial \varphi}{\partial y}\frac{\partial T}{\partial y}\right) + \frac{D_{\mathrm{T}}}{T_\infty}\left[\left(\frac{\partial T}{\partial x}\right)^2 + \left(\frac{\partial T}{\partial y}\right)^2\right]\right\}.\end{aligned} \tag{10}$$

Using the order of magnitude analysis for the y-direction momentum equation which is normal to the stretching sheet and boundary layer approximation [41], such as

$$\begin{aligned}&u \gg v, \\ &\frac{\partial u}{\partial y} \gg \frac{\partial u}{\partial x}, \frac{\partial v}{\partial t}, \frac{\partial v}{\partial x}, \frac{\partial v}{\partial y}, \\ &\frac{\partial p}{\partial y} = 0.\end{aligned} \tag{11}$$

After the analysis, the boundary layer Eqs. (1)–(5) are reduced to the following as:

$$\frac{\partial u}{\partial x} + \frac{\partial v}{\partial y} = 0, \tag{12}$$

$$\begin{aligned}\frac{\partial u}{\partial t} + u\frac{\partial u}{\partial x} + v\frac{\partial u}{\partial y} &= -\frac{1}{\rho_{\mathrm{f}}}\frac{\partial P}{\partial x} + \nu\left(\frac{\partial^2 u}{\partial y^2}\right) + \frac{\sigma}{\rho_{\mathrm{f}}}\left(EB - B^2 u\right) \\ &+ \frac{1}{\rho_{\mathrm{f}}}\left[(1-\varphi_\infty)\rho_{\mathrm{f}\infty}\beta\left(T - T_\infty\right) - \left(\rho_{\mathrm{p}} - \rho_{\mathrm{f}\infty}\right)\left(\varphi - \varphi_\infty\right)\right]g,\end{aligned} \tag{13}$$

$$\begin{aligned}&\frac{\partial T}{\partial t} + u\frac{\partial T}{\partial x} + v\frac{\partial T}{\partial y} \\ &= \frac{k}{(\rho c)_{\mathrm{f}}}\left(\frac{\partial^2 T}{\partial y^2}\right) + \frac{1}{(\rho c)_{\mathrm{f}}}\left(\frac{16T_\infty^3\sigma^*}{3k^*}\frac{\partial^2 T}{\partial y^2}\right) + \frac{\mu}{(\rho c)_{\mathrm{f}}}\left(\frac{\partial u}{\partial y}\right)^2 \\ &+ \tau\left[D_{\mathrm{B}}\left(\frac{\partial \varphi}{\partial y}\frac{\partial T}{\partial y}\right) + \frac{D_{\mathrm{T}}}{T_\infty}\left(\frac{\partial T}{\partial y}\right)^2\right],\end{aligned} \tag{14}$$

$$\begin{aligned}&\frac{\partial \varphi}{\partial t} + u\frac{\partial \varphi}{\partial y} + v\frac{\partial \varphi}{\partial y} \\ &= D_{\mathrm{B}}\left(\frac{\partial^2 \varphi}{\partial y^2}\right) + \frac{D_{\mathrm{T}}}{T_\infty}\left(\frac{\partial^2 T}{\partial y^2}\right) - k_1\left(\varphi - \varphi_\infty\right).\end{aligned} \tag{15}$$

The resulting equations are reduced to the dimensionless form by introducing the following dimensionless quantities.

$$\begin{aligned}&\psi = \sqrt{\frac{b\nu}{1-at}}xf\left(\eta\right), \quad \eta = y\sqrt{\frac{b}{\nu\left(1-at\right)}}, \quad \theta = \frac{T - T_\infty}{T_W - T_\infty}, \\ &\phi = \frac{\varphi - \varphi_\infty}{\varphi_W - \varphi_\infty}, \\ &T_W\left(x,t\right) = T_\infty + T_0\frac{bx}{2\nu(1-at)^2}, \\ &\varphi_W\left(x,t\right) = \varphi_\infty + \varphi_0\frac{bx}{2\nu(1-at)^2}.\end{aligned} \tag{16}$$

The stream function ψ can be defined as:

$$u = \frac{\partial \psi}{\partial y}, \quad v = -\frac{\partial \psi}{\partial x}. \tag{17}$$

Applying Eqs. (16)–(17) into Eqs. (12)–(15), the equations of momentum, energy, and nanoparticle concentration in dimensionless form become:

$$\begin{aligned}&f''' + ff'' - f'^2 - \delta\left(f' + \frac{\eta}{2}f''\right) + M\left(E_1 - f'\right) \\ &+ \lambda\left(\theta - Nr\phi\right) = 0,\end{aligned} \tag{18}$$

$$\begin{aligned}&\frac{1}{Pr}\left(1 + \frac{4}{3}Rd\right)\theta'' + f\theta' - 2f'\theta - \delta\left(\frac{\eta}{2}\theta' + 2\theta\right) \\ &+ Nb\phi'\theta' + Nt\theta'^2 + Ec\left(f''\right)^2 = 0,\end{aligned} \tag{19}$$

$$\begin{aligned}&\phi'' + \frac{Nt}{Nb}\theta'' + Lef\phi' - 2Lef'\phi \\ &- Le\delta\left(\frac{\eta}{2}\phi' + 2\phi\right) - Le\gamma\phi = 0.\end{aligned} \tag{20}$$

The boundary conditions are given as:

$$\begin{aligned}&f = s, \quad f' = 1, \quad \theta = 1, \quad \phi = 1, \quad \text{at} \quad \eta = 0, \\ &f' = 0, \quad \theta = 0, \quad \phi = 0, \quad \text{as}\ \eta \longrightarrow \infty.\end{aligned} \tag{21}$$

Here f, θ, and ϕ are the dimensionless velocity, temperature, and concentration, respectively. As $\delta = a/b$ represents the unsteadiness parameter, $Nr = (\rho_{\mathrm{f}} - \rho_{\mathrm{f}\infty})(\varphi_W - \varphi_\infty)/[\beta(1-\varphi_\infty)\rho_{\mathrm{f}\infty}(T_W - T_\infty)]$ is the buoyancy ratio parameter, $\lambda = Gr/Re^2$ denotes the mixed convection parameter (where $\lambda > 0$ associate with heated surface, $\lambda < 0$ denotes cold surface, and $\lambda = 0$ is the force convection state), $Gr = g\beta(1-\varphi_\infty)\rho_{\mathrm{f}\infty}(T_W - T_\infty)/(\nu^2\rho_{\mathrm{f}})$ is the Grashof number, $Re = bx^2/[\nu(1-at)]$ is the Reynolds number, $Pr = \nu/\alpha$ stand for Prandtl number, $Nb = (\rho c)_{\mathrm{p}}D_{\mathrm{B}}(\varphi_W - \varphi_\infty)/[(\rho c)_{\mathrm{f}}\nu]$ is the Brownian motion parameter, $Le = \nu/D_{\mathrm{B}}$ is the Lewis, $Nt = (\rho c)_{\mathrm{p}}D_{\mathrm{T}}(T_W - T_\infty)/[(\rho c)_{\mathrm{f}}\nu T_\infty]$ is the thermophoresis parameter, $M = \sigma B_0^2/(b\rho_{\mathrm{f}})$ is the magnetic field parameter, $E_1 = E_0/(u_W B_0)$ is the electric field parameter, $Ec = u_W^2/\left[c_{\mathrm{p}}\left(T_W - T_\infty\right)\right]$ is the Eckert number, $s = v_0/\sqrt{\nu b}$ is the suction ($s > 0$) /injection ($s < 0$) parameter, $Rd = 4\sigma^* T_\infty^3/(k^* k)$ is the radiation parameter, $\gamma = k_0/b$ is the chemical reaction ($\gamma > 0$ associates to destructive chemical reaction while $\gamma < 0$ corresponds to generative chemical reaction) respectively. Prime represents differentiation with respect to η. In our present study, the selection of non-dimensional sundry parameters of nanofluids is considered to vary in view of the works [3,8,15,17,19,41,42].

The skin friction coefficient, the local Nusselt number, and the local Sherwood number are

$$\begin{aligned}&c_{\mathrm{f}} = \frac{\tau_W}{\rho u_W^2\left(x,t\right)}, \quad Nu = \frac{xq_W}{k\left(T_W - T_\infty\right)}, \\ &Sh = \frac{xq_m}{D_{\mathrm{B}}\left(\varphi_W - \varphi_\infty\right)},\end{aligned} \tag{22}$$

where

$$q_W = -\left[\left(k + \frac{16\sigma^* T_\infty^3}{3k^*}\right)\frac{\partial T}{\partial y}\right]_{y=0}, \quad q_m = -D_B\left(\frac{\partial \varphi}{\partial y}\right)_{y=0},$$
$$\tau_W = \mu_f\left(\frac{\partial u}{\partial y}\right)_{y=0}. \tag{23}$$

Here τ_W is the shear stress in the stretching surface, q_W is the surface heat flux, while q_m is the surface mass flux, and k is the thermal conductivity of the nanofluid. The local skin-friction coefficient, local Nusselt and local Sherwood numbers are presented in non-dimensional form as

$$Re^{1/2}c_f = f''(0), \quad Nu/Re^{1/2} = -\left(1 + \frac{4}{3}Rd\right)\theta'(0),$$
$$Sh/Re^{1/2} = -\phi'(0). \tag{24}$$

Volumetric analysis due to entropy generation rate of the electrical MHD nanofluid over a stretching sheet consider thermal radiation impacts. Using Roseland approximation approach as discussed in Refs. [13,15], the equation is presented as follow:

$$\begin{aligned} S'''_{gen} = {} & \frac{k}{T_\infty^2}\left[\left(\frac{\partial T}{\partial y}\right)^2 + \frac{16\sigma^* T_\infty^3}{3k^* k}\left(\frac{\partial T}{\partial y}\right)^2\right] \\ & + \frac{\mu}{T_\infty}\left\{2\left[\left(\frac{\partial u}{\partial x}\right)^2 + \left(\frac{\partial v}{\partial y}\right)^2\right] + \left(\frac{\partial u}{\partial y}\right)^2\right\} \\ & + \frac{RD}{\varphi_\infty}\left[\left(\frac{\partial \varphi}{\partial x}\right)^2 + \left(\frac{\partial \varphi}{\partial y}\right)^2\right] \\ & + \frac{RD}{\varphi_\infty}\left[\left(\frac{\partial T}{\partial x}\right)\left(\frac{\partial \varphi}{\partial x}\right) + \left(\frac{\partial T}{\partial y}\right)\left(\frac{\partial \varphi}{\partial y}\right)\right] \\ & + \frac{\sigma}{T_\infty}(uB - E)^2. \end{aligned} \tag{25}$$

The equation above contains the heat transfer irreversibility (conduction effect), fluid friction irreversibility, diffusive and Joule dissipation irreversibility. The first is the entropy generation over heat transfer through finite temperature difference and thermal radiation. Second is the entropy generation due to fluid friction irreversibility, third is due to diffusion which is the total across thermal and concentration gradients and term that has only concentration gradient, and fourth is the Joule dissipation containing the magnetic and electric fields. After implementing the scaling analysis and boundary layer approximation, the dimensionless of entropy generation rate which is the entropy generation number, is the ratio of actual entropy generation S'''_{gen} to the characteristic entropy generation rates S'''_0, can be represented as [36,42]:

$$\begin{aligned} N_G = \frac{S'''_{gen}}{S'''_0} = {} & \left(1 + \frac{4}{3}Rd\right)Re\theta'^2 + \frac{Br}{\Omega}Re(f'')^2 \\ & + Re\zeta\left(\frac{\Sigma}{\Omega}\right)^2\phi'^2 + Re\zeta\left(\frac{\Sigma}{\Omega}\right)\theta'\phi' \\ & + Ha^2\left(\frac{Br}{\Omega}\right)(f' - E_1)^2, \end{aligned} \tag{26}$$

where $S'''_0 = k(T_W - T_\infty)^2/(x^2 T_\infty^2)$ is the characteristic entropy generation rate, $\Omega = (T_W - T_\infty)/T_\infty$ the dimensionless temperature difference, $\Sigma = (\varphi_W - \varphi_\infty)/\varphi_\infty$ the dimensionless concentration difference, $Br = \mu U_W^2/[k(T_W - T_\infty)]$ the Brinkman number, $Ha^2 = \sigma B_0^2 x^2/[(1 - at)\mu]$ the Hartman number, and $\zeta = RD\varphi_\infty/k$ is the diffusion constant parameter entropy parameters, respectively.

The domination of the irreversibility process is of significant interest since the entropy generation rate is unable to solve this problem. Looking at Bejan number, defined as the entropy generation as a result of heat transfer to the total entropy generation, is used to study the entropy generation processes. Bejan number in dimensionless is given as [33,34]:

$$Be = \frac{\left(1 + \frac{4}{3}Rd\right)Re\theta'^2}{N_G}. \tag{27}$$

In our study, the dimensionless form of the momentum, energy, and concentration Eqs. (18)–(20) associated with the boundary condition Eq. (21) is a system of highly nonlinear ordinary differential equations that are solved numerically using implicit finite difference method known as Keller box method [40]. This method is unconditionally stable and has second order accuracy. The grid size $\eta = 0.01$ has been used so that the results are mesh independent. It was seen that satisfaction of the outer boundary conditions is obtained by taking the boundary layer thickness $\eta_\infty = 7$ and the convergence tolerance $\varepsilon = 0.00001$. The maximum value of η_∞ was found for each iteration loop by $\eta_\infty = \eta_\infty + \Delta\eta$. The physical sundry parameters are such as magnetic field M, electric field E_1, unsteadiness parameter δ, mixed convection parameter λ, buoyancy ratio parameter Nr, thermal radiation Rd, Eckert number Ec, suction/blowing parameter s, Prandtl number Pr, Brownian motion parameter Nb, thermophoresis parameter Nt, Lewis number Le and chemical reaction γ. Also, the entropy generation number and Bejan number see Eqs. (26) and (27) with parameters viz. dimensionless temperature difference Ω, dimensionless concentration difference Σ, Brinkman number Br, the diffusion constant parameter ζ, Reynolds number Re, and Hartman number Ha, respectively.

The dimensionless velocity $f'(\eta)$ for various values of parameters such as magnetic field M and electric field E_1 are plotted, see Figs. 2 and 3. It is noticed from Fig. 2 that the velocity of the nanofluid reduces with the intensification of the strength of the magnetic field M. The influence of a transverse magnetic field to an electrically conducting nanofluid provides upsurge to a resistive type force known as the Lorentz force. This force has the propensity to slow down the movement of the nanofluid due to the sheet surface. The magnetic field exerts retarding force on the mixed convection flow which tends to increase the skin friction coefficient within the boundary layer vicinity. Use of a magnetic field affecting the force stream has the inclination to encourage a motive force which reduces the motion of the nanofluid. The influence of electric field parameter is displayed in Fig. 3. As the values of electric field parameter increase, the momentum boundary layer

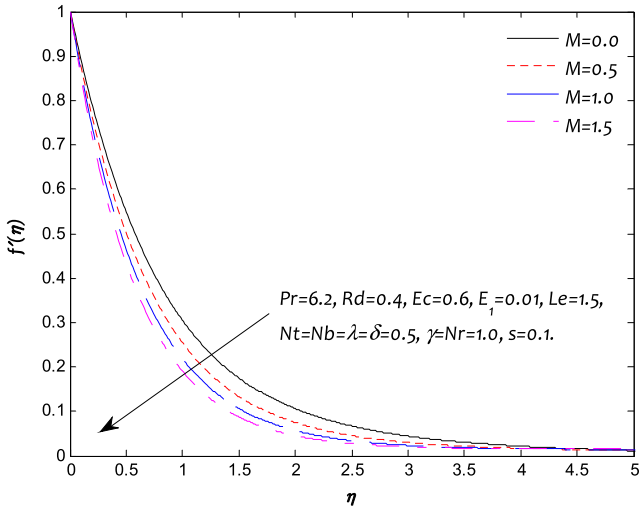

Fig. 2. Influence of M on the velocity profile $f'(\eta)$.

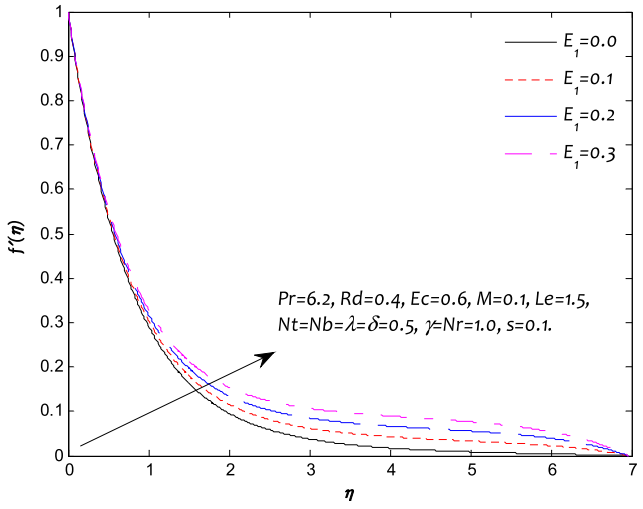

Fig. 3. Influence of E_1 on the velocity profile $f'(\eta)$.

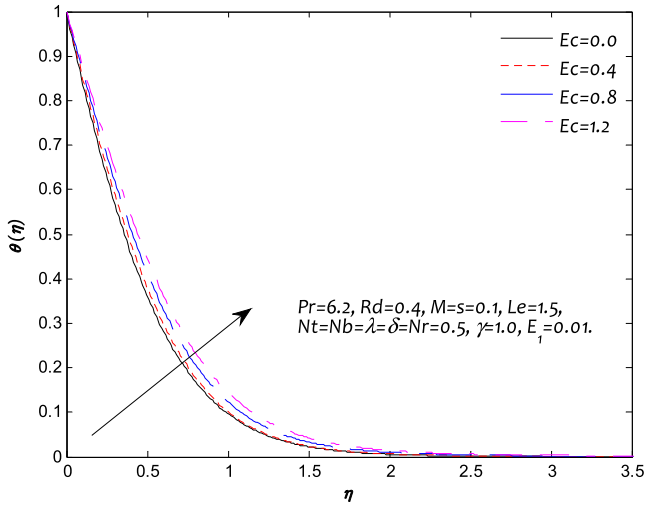

Fig. 5. Influence of Ec on the temperature profile $\theta(\eta)$.

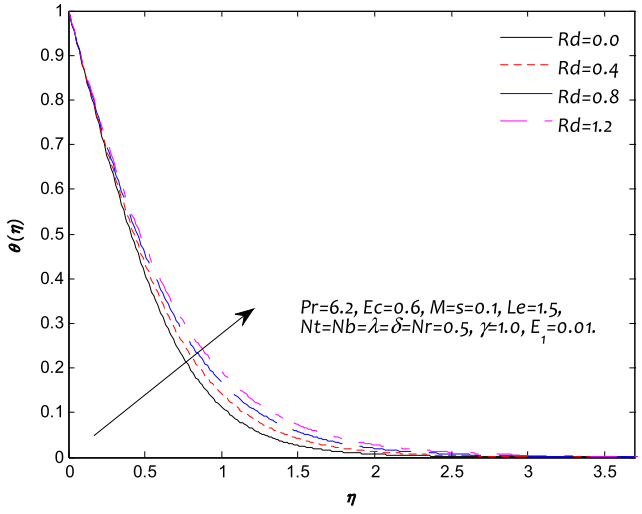

Fig. 4. Influence of Rd on the temperature profile $\theta(\eta)$.

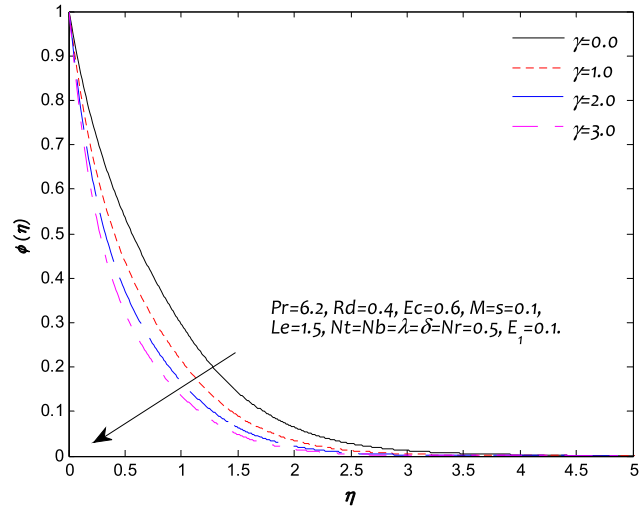

Fig. 6. Influence of γ on the concentration profile $\phi(\eta)$.

rises above the sheet significantly as the skin friction coefficient reduces. Due to Lorentz force rising as result of electric field acts like an accelerating force decreases the frictional resistance which causes to shift the streamline far from the linear stretching surface. This electric field contributes to the thickening of the momentum boundary layer and the accelerating body force to the flow is the cause of enhancing the nanofluid velocity.

The variation in the dimensionless temperature field $\theta(\eta)$ associated with various values of thermal radiation parameter Rd and Eckert number Ec are examined in the Figs. 4 and 5. In Fig. 4, we noticed that higher temperature and thicker thermal boundary layer are associated with larger thermal radiation parameter. The larger radiation gives a significant amount of heat to the fluid as a result of enhancement in the temperature field. The influence of Eckert number is displayed in Fig. 5. The effects of Eckert number is to increase the temperature and boundary layer thickness due to the frictional heating. For low-speed fluid, the viscous dissipation can be ignored.

The effects of chemical reaction parameter γ on the concentration field $\phi(\eta)$ are shown in Fig. 6. It is evident that stronger γ leads to the reduction in nanoparticle concentration and solutal boundary layer thickness. The description of this actions is that the destructive chemical rate ($\gamma > 0$) enhances the mass transfer rate and consequently a reduction in nanoparticle concentration.

Figs. 7 and 8 depict graphical presentations for the entropy generation number as a function of Hartmann number Ha, and dimensionless group $Br\Omega^{-1}$ (that is the ratio of the Brinkman number to the dimensionless to temperature difference). Fig. 7 depicts effects of Hartmann number on the entropy generation number. Entropy generation is sensitive to increase in Hartmann number, because the interaction and action between the electric and magnetic fields strengthen the dissipation energy to thermal diffusion and nanofluid friction. The nanofluid dynamic viscosity reduces, the inter-molecular force binding the fluid nanoparticles gets weaker. Consequently, the level of entropy generation rises as a result of heat transfer from the nanofluid to the stretching sheet and the viscous dissipation due to an interaction of the nanoparticles in the distribution. In Fig. 8, behavior of the dimensionless groups $Br\Omega^{-1}$ on entropy generation number profile is displayed. This dimensionless group is sensitive to an increase in nanofluid friction which results in enhancement in the entropy generation. They are increasing function with entropy generation number, due to mass transfer to the entropy generation number.

Figs. 9 and 10 display the effects of mixed convection parameter λ and buoyancy ratio parameter Nr on Bejan number profiles.

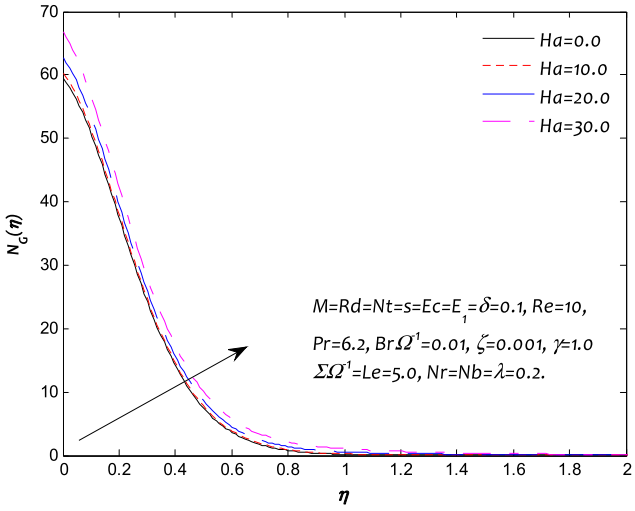

Fig. 7. Influence of Ha on the entropy generation number profile $N_G(\eta)$.

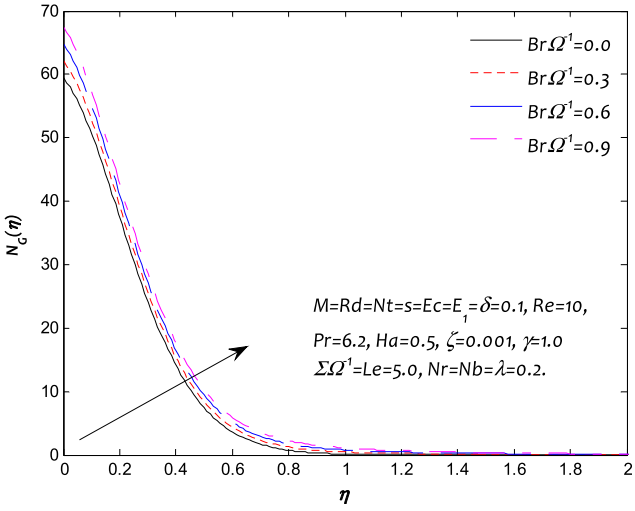

Fig. 8. Influence of $Br\,\Omega^{-1}$ on the entropy generation number profile $N_G(\eta)$.

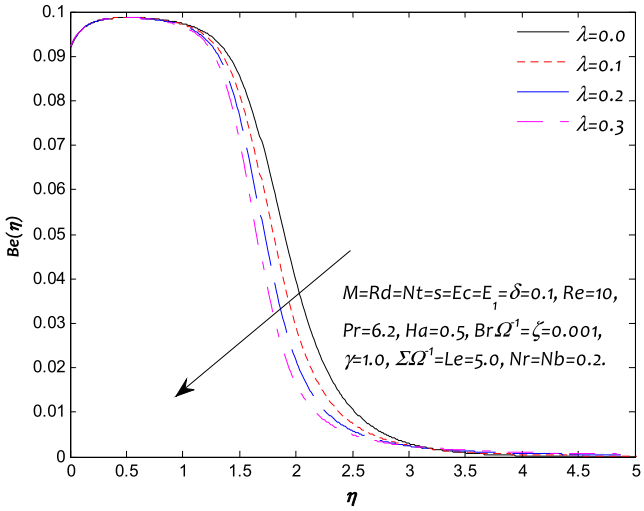

Fig. 9. Influence of λ on the Bejan number profile $Be(\eta)$.

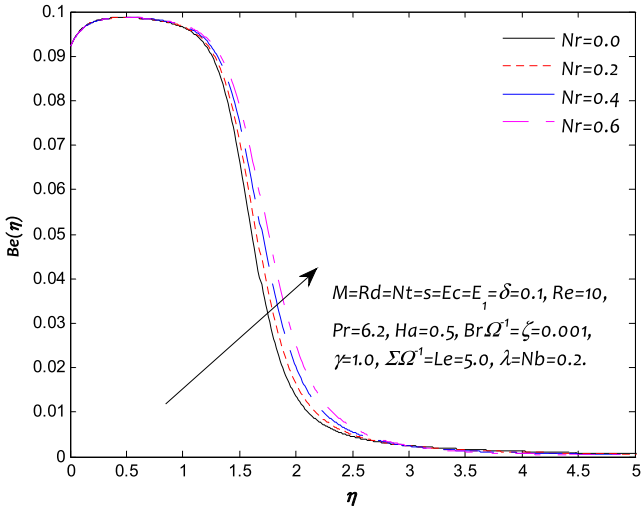

Fig. 10. Influence of Nr on the Bejan number profile $Be(\eta)$.

The influences of mixed convection parameter and Buoyancy ratio parameter on Bejan number profile have reverse effects (see Figs. 9 and 10). Fig. 9 displays the effects of mixed convection parameter λ on the Bejan number profile. For an increase in ($\lambda > 0$) associated with assisting flow reduces as the inertial forces dominate the buoyancy forces away from the sheet. The irreversibility due to mixed convection dominates over the thermal energy near the linear stretching sheet. This resulted in a reduction in the nanofluid and then decrease along the stretching sheet. $\lambda = 0$ signifies force convection flow. The effect of the buoyancy ratio parameter Nr on the Bejan number profile is illustrated in Fig. 10. Higher values of the buoyancy ratio lead to an increase and thereafter decrease near the linear stretching. The irreversibility due to buoyancy ratio dominates the heat transfer close to the wall. This is due to the result of a significant amount of thermal buoyancy forces over the concentration buoyancy forces which dominate the vicinity of the boundary layer region. Due to the dependence of nanofluid on temperature and concentration, heat and mass transfer dominate over thermal diffusion.

The unsteady electrical MHD mixed convection flow and heat transfer of nanofluid due to entropy generation with combined effects of thermal radiation, viscous dissipation, and chemical reaction alongside with wall mass transfer due to linear stretching sheet have been studied. The influences of the involved parameters on the electrical conduction of nanofluid via the velocity, temperature, nanoparticle concentration, entropy generation, and Bejan number are investigated and analyzed with graphical representations. The conclusions are as follows:

1. Velocity field rises with an increase in the electric field but decreases with magnetic field parameter.
2. Temperature field is sensitive to an increase in the thermal radiation and Eckert number.
3. Entropy generation is penetrating to an intensification in Hartmann number and dimensionless group (that is the ratio of the Brinkman number to the dimensionless to temperature difference).
4. Higher values of chemical reaction leading to a reduction in nanoparticle concentration.
5. Buoyancy ratio and mixed convection parameter exhibit an opposite behavior with Bejan number.

Acknowledgments

This research is being supported by the research grant under the Ministry of Higher Education (MOHE), the Fundamental Research Grant Scheme (FRGS) project vote number R.J 130000.7809.4F354.

References

[1] S. Choi, Enhancement Thermal Conductivity of Fluids with Nanoparticles, ASME Publications, 1995.
[2] A. Kuznetsov, D. Nield, Natural convective boundary-layer flow of a nanofluid past a vertical plate, Int. J. Therm. Sci. 49 (2010) 243–247.
[3] W. Khan, I. Pop, Boundary-layer flow of a nanofluid past a stretching sheet, Int. J. Heat Mass Transfer 53 (2010) 2477–2483.
[4] Z. Haddad, E. Abu-Nada, H.F. Oztop, et al., Natural convection in nanofluids: are the thermophoresis and brownian motion effects significant in nanofluid heat transfer enhancement?, Int. J. Therm. Sci. 57 (2012) 152–162.
[5] T. Hayat, M. Imtiaz, A. Alsaedi, et al., Effects of homogeneous–heterogeneous reactions in flow of magnetite-Fe_3O_4 nanoparticles by a rotating disk, J. Molecular Liquids 216 (2016) 845–855.
[6] M. Sheikholeslami, M. Rashidi, T. Hayat, et al., Free convection of magnetic nanofluid considering MFD viscosity effect, J. Molecular Liquids 218 (2016) 393–399.
[7] M. Sheikholeslami, D. Ganji, Nanofluid convective heat transfer using semi analytical and numerical approaches: A review, J. Taiwan Inst. Chem. Eng. 65 (2016) 43–77.
[8] S. Das, R. Jana, O. Makinde, Mixed convective magnetohydrodynamic flow in a vertical channel filled with nanofluids, Int. J. Eng. Sci. Technol. 18 (2015) 244–255.
[9] M. Farooq, M.I. Khan, M. Waqas, et al., MHD stagnation point flow of viscoelastic nanofluid with non-linear radiation effects, J. Molecular Liquids 221 (2016) 1097–1103.
[10] Z. Hedayatnasab, F. Abnisa, W.M.A.W. Daud, Review on magnetic nanoparticles for magnetic nanofluid hyperthermia application, Mater. Des. 123 (2017) 174–196.
[11] J. Gómez-Pastora, S. Dominguez, E. Bringas, et al., Review and perspectives on the use of magnetic nanophotocatalysts (MNPCs) in water treatment, Chem. Eng. J. 310 (2017) 407–427.
[12] M. Sheikholeslami, R. Ellahi, Three dimensional mesoscopic simulation of magnetic field effect on natural convection of nanofluid, Int. J. Heat Mass Transfer 89 (2015) 799–808.
[13] Y.S. Daniel, S.K. Daniel, Effects of buoyancy and thermal radiation on mhd flow over a stretching porous sheet using homotopy analysis method, Alexandria Eng. J. 54 (2015) 705–712.
[14] Y.S. Daniel, Laminar convective boundary layer slip flow over a flat plate using homotopy analysis method, J. Inst. Eng. E 97 (2016) 115–121.
[15] Y.S. Daniel, Z.A. Aziz, Z. Ismail, et al., Effects of thermal radiation, viscous and Joule heating on electrical MHD nanofluid with double stratification, Chinese J. Phys. 55 (2017) 630–651.
[16] N. Freidoonimehr, M.M. Rashidi, S. Mahmud, Unsteady MHD free convective flow past a permeable stretching vertical surface in a nano-fluid, Int. J. Therm. Sci. 87 (2015) 136–145.
[17] M. Hamad, I. Pop, Unsteady MHD free convection flow past a vertical permeable flat plate in a rotating frame of reference with constant heat source in a nanofluid, Heat Mass Transfer 47 (2011) 1517.
[18] M.S. Khan, I. Karim, L.E. Ali, et al., Unsteady MHD free convection boundary-layer flow of a nanofluid along a stretching sheet with thermal radiation and viscous dissipation effects, Int. Nano Lett. 2 (2012) 24.
[19] S. Khalili, S. Dinarvand, R. Hosseini, et al., Unsteady MHD flow and heat transfer near stagnation point over a stretching/shrinking sheet in porous medium filled with a nanofluid, Chin. Phys. B 23 (2014) 048203.
[20] T. Hayat, S. Qayyum, M. Imtiaz, et al., Comparative study of silver and copper water nanofluids with mixed convection and nonlinear thermal radiation, Int. J. Heat Mass Transfer 102 (2016) 723–732.
[21] T. Hayat, S. Qayyum, A. Alsaedi, et al., Inclined magnetic field and heat source/sink aspects in flow of nanofluid with nonlinear thermal radiation, Int. J. Heat Mass Transfer 103 (2016) 99–107.
[22] M. Sheikholeslami, M. Mustafa, D.D. Ganji, Effect of Lorentz forces on forced-convection nanofluid flow over a stretched surface, Particuology 26 (2016) 108–113.
[23] T. Hayat, M. Imtiaz, A. Alsaedi, et al., MHD three-dimensional flow of nanofluid with velocity slip and nonlinear thermal radiation, J. Magn. Magn. Mater. 396 (2015) 31–37.
[24] M. Sheikholeslami, S. Soleimani, D. Ganji, Effect of electric field on hydrothermal behavior of nanofluid in a complex geometry, J. Molecular Liquids 213 (2016) 153–161.
[25] M. Sheikholeslami, A.J. Chamkha, Electrohydrodynamic free convection heat transfer of a nanofluid in a semi-annulus enclosure with a sinusoidal wall, Numer. Heat Transfer A 69 (2016) 781–793.
[26] Y.S. Daniel, Presence of heat generation/absorption on boundary layer slip flow of nanofluid over a porous stretching sheet, American J. of Heat and Mass Transfer 2 (2015) 15.
[27] Y.S. Daniel, MHD laminar flows and heat transfer adjacent to permeable stretching sheets with partial slip condition, J. Adv. Mech. Eng. 4 (2017) 1–15.
[28] Y.S. Daniel, Steady MHD boundary-layer slip flow and heat transfer of nanofluid over a convectively heated of a non-linear permeable sheet, J. Adv. Mech. Eng. 3 (2016) 1–14.
[29] Y.S. Daniel, Steady MHD laminar flows and heat transfer adjacent to porous stretching sheets using HAM, Am. J. Heat Mass Transfer 2 (2015) 146–159.
[30] M. Hamad, M. Ferdows, Similarity solution of boundary layer stagnation-point flow towards a heated porous stretching sheet saturated with a nanofluid with heat absorption/generation and suction/blowing: A Lie group analysis, Commun. Nonlinear Sci. Numer. Simul. 17 (2012) 132–140.
[31] A.U. Rehman, R. Mehmood, S. Nadeem, Entropy analysis of radioactive rotating nanofluid with thermal slip, Appl. Therm. Eng. 112 (2017) 832–840.
[32] M. Mehrali, E. Sadeghinezhad, A.R. Akhiani, et al., Heat transfer and entropy generation analysis of hybrid graphene/ Fe_3O_4 ferro-nanofluid flow under the influence of a magnetic field, Powder Technol. 308 (2017) 149–157.
[33] S.O. Adesanya, O.D. Makinde, Irreversibility analysis in a couple stress film flow along an inclined heated plate with adiabatic free surface, Physica A 432 (2015) 222–229.
[34] A. Eegunjobi, O. Makinde, Irreversibility analysis of hydromagnetic flow of couple stress fluid with radiative heat in a channel filled with a porous medium, Results Phys. 7 (2017) 459–469.
[35] N. Ranjit, G. Shit, Entropy generation on electro-osmotic flow pumping by a uniform peristaltic wave under magnetic environment, Energy 128 (2017) 649–660.
[36] A. López, G. Ibáñez, J. Pantoja, et al., Entropy generation analysis of MHD nanofluid flow in a porous vertical microchannel with nonlinear thermal radiation, slip flow and convective-radiative boundary conditions, Int. J. Heat Mass Transfer 107 (2017) 982–994.
[37] T. Tharayil, L.G. Asirvatham, M.J. Dau, et al., Entropy generation analysis of a miniature loop heat pipe with graphene–water nanofluid: Thermodynamics model and experimental study, Int. J. Heat Mass Transfer 106 (2017) 407–421.
[38] M. Torabi, M. Torabi, S. Ghiaasiaan, et al., The effect of Al_2O_3-water nanofluid on the heat transfer and entropy generation of laminar forced convection through isotropic porous media, Int. J. Heat Mass Transfer 111 (2017) 804–816.
[39] F. Mabood, W. Khan, A.M. Ismail, Mhd boundary layer flow and heat transfer of nanofluids over a nonlinear stretching sheet: a numerical study, J. Magn. Magn. Mater. 374 (2015) 569–576.
[40] T. Cebeci, P. Bradshaw, Physical and Computational Aspects of Convective Heat Transfer, Springer Science & Business Media, 2012.
[41] W. Ibrahim, B. Shankar, MHD boundary layer flow and heat transfer of a nanofluid past a permeable stretching sheet with velocity, thermal and solutal slip boundary conditions, Comput. & Fluids 75 (2013) 1–10.
[42] A. Noghrehabadi, M.R. Saffarian, R. Pourrajab, et al., Entropy analysis for nanofluid flow over a stretching sheet in the presence of heat generation/absorption and partial slip, J. Mech. Sci. Technol. 27 (2013) 927–937.